ACS Catalysis

Research Article

pubs.acs.org/acscatalysis

Platinum–Ruthenium Nanotubes and Platinum–Ruthenium Coated Copper Nanowires As Efficient Catalysts for Electro-Oxidation of Methanol

Jie Zheng,[†] David A. Cullen,[‡] Robert V. Forest,[†] Jarrid A. Wittkopf,[†] Zhongbin Zhuang,[†] Wenchao Sheng,[†,§] Jingguang G. Chen,[§] and Yushan Yan*[,†]

[†]Department of Chemical and Biomolecular Engineering, University of Delaware, 150 Academy Street, Newark, Delaware 19716, United States

[‡]Oak Ridge National Laboratory, 1 Bethel Valley Road, Oak Ridge, Tennessee 37931, United States

[§]Department of Chemical Engineering, Columbia University, 500 West 120th Street, New York, New York 10027, United States

Supporting Information

ABSTRACT: The sluggish kinetics of methanol oxidation reaction (MOR) is a major barrier to the commercialization of direct methanol fuel cells (DMFCs). In this work, we report a facile synthesis of platinum–ruthenium nanotubes (PtRuNTs) and platinum–ruthenium-coated copper nanowires (PtRu/CuNWs) by galvanic displacement reaction using copper nanowires as a template. The PtRu compositional effect on MOR is investigated; the optimum Pt/Ru bulk atomic ratio is about 4 and surface atomic ratio about 1 for both PtRuNTs and PtRu/CuNWs. Enhanced specific MOR activities are observed on both PtRuNTs and PtRu/CuNWs compared with the benchmark commercial carbon-supported PtRu catalyst (PtRu/C, Hispec 12100). X-ray photoelectron spectroscopy (XPS) reveals a larger extent of electron transfer from Ru to Pt on PtRu/CuNWs, which may lead to a modification of the d-band center of Pt and consequently a weaker bonding of CO (the poisoning intermediate) on Pt and a higher MOR activity on PtRu/CuNWs.

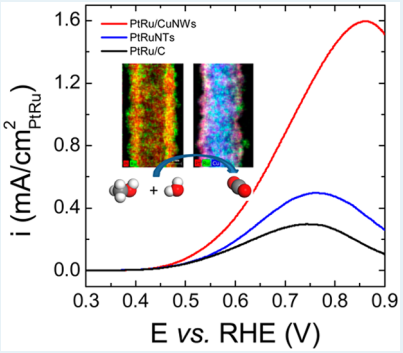

KEYWORDS: *methanol fuel cells, electrocatalysis, methanol oxidation reaction, one-dimensional structure, platinum–ruthenium*

INTRODUCTION

Direct methanol fuel cells (DMFCs) are an attractive alternative to hydrogen-fueled proton exchange membrane fuel cells (PEMFCs) for powering portable devices because of their high energy density (4.8 kWh/L) and ease of fuel transportation and storage.[1,2] However, in practice, DMFCs exhibit low energy density and efficiency due to the sluggish methanol oxidation reaction (MOR) (which leads to a large overpotential) and the crossover of methanol from anode to cathode.[3] Tremendous efforts have been devoted to the development of novel MOR catalysts in the past few decades in order to lower the anode overpotential, and PtRu alloys are recognized as the most active catalyst so far.[4,5] However, even with the state-of-art PtRu catalysts (carbon-supported PtRu nanoparticles or PtRu/C), the MOR activity is still not high enough: an anode overpotential of about 350 mV exists which needs to be reduced.

One-dimensional (1D) nanostructures with extended surfaces such as nanowires, nanotubes, and nanorods usually have a preferential exposure of certain facets which may enhance their catalytic MOR activities because MOR is well-known to be structure sensitive.[6] Koenigsmann et al. gave a detailed review on 1D noble metal catalysts as a promising structure paradigm for both MOR and oxygen reduction reaction in DMFCs.[7] Studies have shown that Pt nanotubes (PtNTs),[8] porous Pt nanotubes (porous-PtNTs),[9] and ultrathin Pt nanowires (PtNWs)[10] all exhibited improved MOR activity over supported Pt nanoparticles (Pt/C). One-dimensional Pt alloy nanostructures, such as PtNi nanotubes,[11] PtNiP composite nanotubes,[12] PtPd nanotubes, and nanorods,[13] PtFe and PtPdFe nanowires,[14] PtRu nanowires,[15,16] PtPdTe nanowires,[17] and Au/Pt and Au/PtCu nanowires,[18] have also been demonstrated to be better MOR catalysts, attributed to bifunctional mechanisms[19,20] or electronic effects[21] of the Pt alloy systems. In addition to the improved MOR activity, 1D nanostructures are believed to have the potential to enhance mass transport in the electrode during fuel cell operation.[15] Among various alloying elements, Ru is still the best choice in improving the MOR kinetics. Benefiting from the advantages of 1D structure and the promotional effect of Ru, 1D PtRu nanostructures are of great interest but work in this area has been limited. The reported 1D PtRu nanostructures were synthesized by template-assisted electrodeposition using AAO[22] or SBA-15[15] as hard template followed by template removal or

Received: September 23, 2014
Revised: January 10, 2015
Published: January 15, 2015

DOI: 10.1021/cs501449y
ACS Catal. 2015, 5, 1468–1474

by electrodeposition of PtRu on Au-coated ZnO-NTs.[23] Their MOR activities are similar or slightly higher than that of PtRu/C. Additionally, these methods usually are only suitable for small scale synthesis, and the yield is low. Alternatively, galvanic displacement reactions were widely used for synthesizing noble metal materials using less noble metal as template, such as Ag,[24−26] Cu,[27−30] and Te.[17,31,32]

Herein we report a simple galvanic displacement method to generate PtRuNTs and PtRu/CuNWs as efficient MOR catalysts. CuNWs were used as template and were synthesized by reduction of copper nitrate with hydrazine and ethylenediamine.[33] PtRuNTs and PtRu/CuNWs were prepared by complete and partial galvanic displacing Cu with Pt and Ru, respectively. (See the Experimental Section for details.) By varying the Pt and Ru precursor ratio, PtRuNTs and PtRu/CuNWs with different Pt/Ru ratios were obtained. PtRuNTs and PtRu/CuNWs showed higher MOR activities than the benchmark commercial PtRu/C catalyst (Johnson Matthey Hispec 12100, 50 wt % Pt, 25 wt % Ru on high surface area advanced carbon support).

EXPERIMENTAL SECTION

Synthesis of CuNWs. CuNWs were synthesized by reduction of copper nitrate trihydrate ($Cu(NO_3)_2{\cdot}3H_2O$, Sigma-Aldrich) with hydrazine (N_2H_4, 35 *wt.* % solution in water, Aldrich) in an aqueous sodium hydroxide (NaOH, Fisher Chemical) solution in the presence of ethylenediamine (EDA, ≥ 99.5%, Fluka). In a typical CuNW synthesis, 200 mg $Cu(NO_3)_2$ in 10 mL of DI H_2O was added to 200 mL of 10 M NaOH in a 500 mL glass bottle. EDA (1.5 mL) and N_2H_4 (0.25 mL) were subsequently added to the solution. The glass bottle was capped after the addition of all the components and shaken vigorously to ensure complete mixing. Then the bottle was heated in a 65 °C water bath for 1 h. The product was collected by filtration and washed with DI water until the pH of the filtrate reached 7. The filter cake was stored in a desiccator, dried overnight, and collected for future use.

Synthesis of PtRuNTs and PtRu/CuNWs. PtRuNTs and PtRu/CuNWs were synthesized by complete and partial galvanic displacement of CuNWs. In a typical synthesis, CuNWs (20 mg) were dispersed in 400 mL of water and added into a 1 L three-neck round-bottom flask with a stir bar inside. Various amounts of chloroplatnic acid ($H_2PtCl_6{\cdot}xH_2O$, Aldrich) and ruthenium chloride ($RuCl_3{\cdot}xH_2O$, Aldrich) in 100 mL of water were prepared in a dropping funnel and added dropwise in a dropping rate of about 2 s per drop to the CuNWs suspension after flowing Ar for 15 min. The reaction continued for 1 h at room temperature to ensure a complete reaction. After the synthesis, the products were collected by filtration and washed with copious amounts of DI water. The products were stored in a desiccator under vacuum, dried overnight, and collected for characterization. All the PtRuNTs samples were annealed at 250 °C in a tube furnace for 2 h in Ar, whereas all the PtRu/CuNWs were not.

Electron Microscopy Characterization. The morphology of synthesized CuNWs, PtRuNTs and PtRu/CuNWs were characterized by scanning electron microscopy (SEM, JSM-7400F) and transmission electron microscopy (TEM, JEM-2010F). TEM samples were prepared on a lacey carbon copper grid by adding a drop of sample water suspension on top. The compositional ratio was studied by electron dispersive X-ray spectroscopy (EDS) on SEM. The elemental mappings of PtRuNTs and PtRu/CuNWs were obtained by scanning transmission electron microscopy (STEM), specimens were prepared by sonicating the nanowires in methanol, then drop casting the solution onto lacey carbon-coated Au grids. Energy dispersive X-ray spectroscopy (EDS) spectrum imaging was performed in a Hitachi 3300 equipped with a 60 mm^2 Bruker X-flash detector, as well as secondary electron (SE) and high-angle annular dark-field (HAADF) detectors for image capture. Higher-resolution STEM images were recorded in an aberration-corrected JEOL 2200FS.

X-ray Diffraction and X-ray Photoelectron Spectroscopy. X-ray diffraction (XRD) patterns were recorded on a Philips X'Pert X-ray diffractometer using Cu Kα radiation. X-ray photoelectron spectroscopy (XPS) measurements were performed using a Physical Electronics 5600 series XPS system equipped with a multichannel hemispherical analyzer and Mg anode X-ray source. The binding energy scale was calibrated by comparing the primary photoelectron peaks of Au, Ag, and Cu reference foils to values published in literature. Sample charging was corrected by setting the binding energy of the C 1s peak to 284.8 eV.

Electrochemical Measurements. The electrochemical measurements were conducted using a three-electrode cell configuration, with silver/silver chloride electrode (Ag/AgCl) as the reference electrode, Pt wire as the counter electrode, and a 5 mm diameter glassy carbon electrode (PINE instruments) as working electrode on a multichannel potentiostat (Princeton Applied Research). All the potentials used in this work were referred to that of the reversible hydrogen electrode (RHE).

The thin-film electrodes were prepared by pipetting 20 μL of catalyst ink (catalyst ultrasonically dispersed in water) onto glassy carbon electrodes which had been prepolished to a mirror finish. The final precious metal loading for PtRuNTs is 100 $\mu g_{PtRu}/cm^2_{disk}$, and that for PtRu/CuNWs is about 25−30 $\mu g_{PtRu}/cm^2_{disk}$. Cyclic voltammetry (CV) experiments were performed in 0.1 M $HClO_4$ solution with 1 M CH_3OH at a scanning rate of 5 mV/s in an Ar atmosphere. A small scanning rate of 5 mV/s was used in order to minimize the contribution of current from CV without methanol as well as to give the system enough time to achieve steady state during the sweeping of potential. The voltammogram curves were recorded in the potential region of 0.02 to 0.9 V vs RHE.

CO stripping was used to determine the surface areas as well as the CO tolerance properties of Pt and PtRu catalysts. In a CO-stripping test, the electrode potential was held at 0.1 V vs RHE for 10 min for a fully adsorption of CO on the catalyst surface followed by flowing Ar for another 10 min to remove the CO in the electrolyte. The first positive scan shows the stripping of a monolayer of CO while a second scan will be used to judge whether the adsorbed CO has been completely oxidized in the first scan. The oxidation charge of CO stripping (Q_{CO}) was calculated by integrating the area under CO-stripping curve with subtraction of CV curve in the second scan, and the electrochemical surface areas (ECSAs) were calculated using eq 1. The oxidation charge for removing one monolayer of CO was assumed to be 420 $\mu C/cm^2$ on PtRu surfaces.

$$\mathrm{ECSA} = \frac{Q_{CO}}{420\mu C/cm^2} \quad (1)$$

DOI: 10.1021/cs501449y
ACS Catal. 2015, 5, 1468−1474

RESULTS AND DISCUSSION

CuNWs (Figure S1) with diameters in the range of 80−110 nm and lengths in the range of 20−40 μm were synthesized and used as the template to generate PtRuNTs and PtRu/CuNWs. PtRuNTs and PtRu/CuNWs with different Pt/Ru atomic ratios were prepared and termed as PtRu(1-1)NTs, PtRu(3-1)NTs, PtRu(6-1)NTs, PtRu(9-1)NTs, PtRu(1-1)/CuNWs, PtRu(3-1)/CuNWs, PtRu(4-1)/CuNWs, PtRu(6-1)/CuNWs, and PtRu(9-1)/CuNWs. (The number in the parentheses indicates the bulk Pt/Ru atomic ratio measured by EDX in SEM.) Their SEM images are shown in Figure S2 and S5. The elemental compositions of all samples were measured by energy dispersive X-ray spectrospcopy (EDX) (Figure S3 and S6), and the results were listed in Table S1, where we can see that all PtRuNTs samples had a residual copper content of about 5−9 wt %, whereas all PtRu/CuNWs samples had a copper content of about 70−75 wt %.

The SEM and TEM images of PtRu(6-1)NTs (Figure 1a,c) show clear hollow tube structures which was caused by the so-

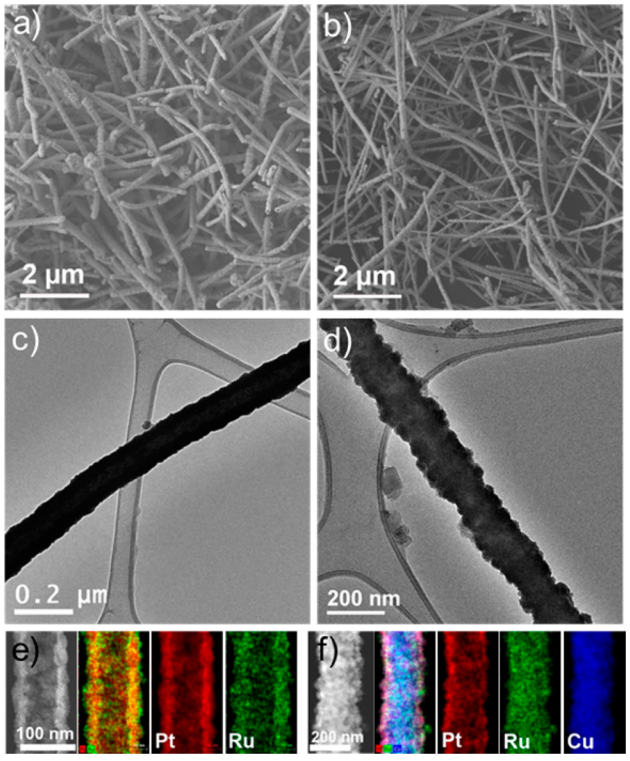

Figure 1. SEM and TEM images of (a,c) PtRu(6-1)NTs and (b,d) PtRu(4-1)/CuNWs; HAADF-STEM image and corresponding elemental spectrum images of a (e) PtRu(6-1)NT; and (f) PtRu(4-1)/CuNW with Pt shown in red, Ru in green, and Cu in blue.

called "Kirkendall Effect".[34,35] The diameter of PtRuNTs is about 120 nm, and the nanotube wall thickness is about 30 nm. The length of PtRuNTs shrinks to about 6−10 μm due to cracking during the galvanic displacement reaction. The PtRu(4-1)/CuNWs have a diameter of about 120 nm and length of around 10 μm (Figure 1b,d). The weight percentage of precious metals (Pt and Ru) in all PtRu/CuNWs is 25−30 wt % (Table S1), which is about 1/3 of that in PtRuNTs. The shell thicknesses of PtRu/CuNWs is estimated to be 10−20 nm (e.g., Figure S7 for PtRu(4-1)/CuNWs). The high-angle angular dark-field scanning transmission electron microscopy (HAADF-STEM) images of a typical PtRu(6-1)NT and PtRu(4-1)/CuNW and the corresponding elemental spectrum images are shown in Figure 1e,f. A hollow structure of a PtRu(6-1)NT can be clearly seen in Figure 1e and also in the cross-sectional view of a PtRu(6-1)NT (Figure S4a−d). The line scan along the tube (Figure S4e) clearly demonstrates the existence of a hollow structure. Figure 1f confirms that PtRu/CuNWs have a Cu-rich core, PtRu-rich shell structure. This can also be seen from the cross-sectional view and line scan of a PtRu(4-1)/CuNW (Figure S7).

The X-ray diffraction (XRD) patterns show that the CuNWs (Figure 2a) have a face-centered cubic (fcc) structure (SG:

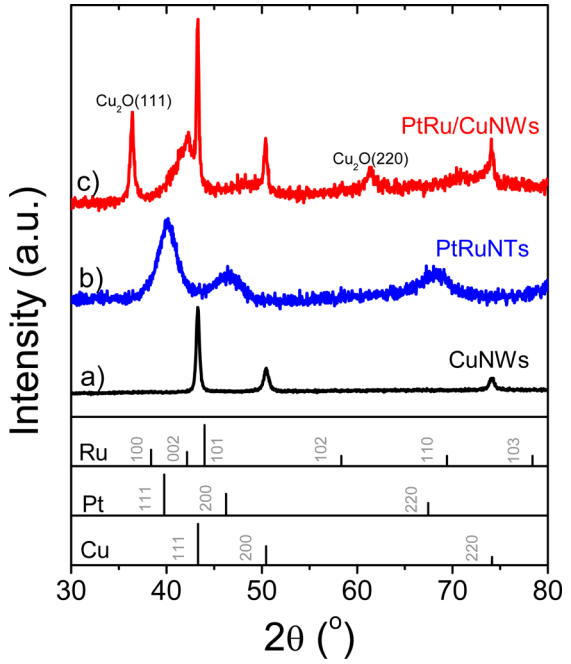

Figure 2. X-ray diffraction patterns of PtRu(4-1)/CuNWs, PtRu(6-1)NTs, and CuNWs.

$Fm\bar{3}m$; JCPDS card no. 04-0836) and the PtRuNTs (Figure 2b) also possess a fcc strcuture with characteristic diffraction peaks of Pt(111), Pt(200), and Pt(220). The Pt peaks shift to higher 2θ angles than pure Pt, reflecting a lattice contraction due to the partial substitution of Pt by Ru to form a PtRu alloy. In the case of PtRu/CuNWs (Figure 2c), the three narrow Cu peaks at 2θ angles of 43.4°, 50.4°, and 74.1° are due to the presence of a pure copper core. The broad peak at 42.3° is from PtRuCu alloys formed on the surface. The formation of surface alloy during galvanic displacement reaction was also reported in literature to be essential for maintaining the original template structures.[36] The two peaks at 36.4° and 61.4° can be attributed to $Cu_2O(111)$ and $Cu_2O(220)$ largely due to the oxidation of surface copper during sample handling and storage. Upon increasing the amount of Pt and Ru precursors, as in the case of PtRuNTs, the Cu_2O peaks disappeared. This phenomenon was also observed in the synthesis of CuPd and CuPt nanotubes using galvanic displacement reaction.[28] The XRD patterns of PtRuNTs and PtRu/CuNWs with other Pt/Ru ratios were very similar to the ones shown here.

Because Ru oxidation occurs at about 0.25 V vs NHE, which overlaps with the hydrogen oxidation reign (0−0.3 V),[37] it is not suitable to use hydrogen adsorption and desorption peaks to determine the electrochemical active surface area (ECSA) of

DOI: 10.1021/cs501449y
ACS Catal. 2015, 5, 1468−1474

a PtRu sample. Hence, CO-stripping voltammetry[38] is adopted to obtain the ECSA of all PtRu samples in this work. The ECSAs determined from CO stripping of PtRu(4-1)/CuNWs, PtRu(6-1)NTs, and PtRu/C (Figure 3) are 29.0 ± 2.4 m^2/g_{PtRu}, 9.4 ± 0.9 m^2/g_{PtRu}, and 73.6 ± 5.1 m^2/g_{PtRu}, respectively. PtRu(4-1)/CuNWs have an ECSA about three times that of PtRu(6-1)NTs. CO-stripping voltammograms also reveal the relative anti-CO poisoning properties of PtRu/CuNWs, PtRuNTs and PtRu/C. Although PtRu(4-1)/CuNWs have a CO-stripping peak potential at about 0.56 V, which is higher than those of PtRu(6-1)NTs (0.54 V) and PtRu/C (0.54 V), PtRu(4-1)/CuNWs exhibit a lower onset potential (0.28 V) for CO monolayer oxidation than PtRu(6-1)NTs (0.30 V) and PtRu/C (0.32 V). (The onset potentials are determined at the potential when the specific current is 0.03 $\mu A/cm^2_{PtRu}$.) The higher CO-stripping peak potential of PtRu/CuNWs might be caused by the presence of surface copper. When we compare the CO-stripping peak potential of Pt/CuNWs and PtNTs (Figure S13b), Pt/CuNWs showed a higher peak potential than PtNTs.

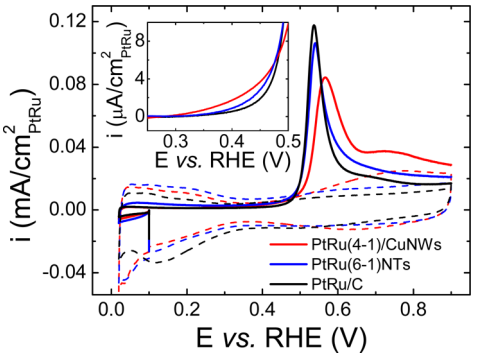

Figure 3. CO-stripping voltammograms (solid lines) and cyclic voltammograms (dash lines) of PtRu(4-1)/CuNWs, PtRu(6-1)NTs, and PtRu/C in 0.1 M $HClO_4$, 20 mV/s, CO was preadsorbed at 0.1 V vs RHE for 10 min followed by Ar-purging for another 10 min, inset: close-up image of CO-stripping curves in 0.25−0.5 V vs RHE. Currents are normalized to true PtRu surface area determined from CO stripping.

The MOR activities of PtRu(6-1)NTs and PtRu(4-1)/CuNWs and PtRu/C were investigated. PtRu(6-1)NTs have a peak MOR specific current density (0.5 mA/cm^2_{PtRu}) 1.7 times that of PtRu/C (0.29 mA/cm^2_{PtRu}) (Figure 4a). However, PtRu(6-1)NTs show much smaller mass activity than PtRu/C (Figure 4b), attributed to their small ECSA. PtRu(4-1)/CuNWs exhibit much higher specific activity: its peak current density (1.6 mA/cm^2_{PtRu}) is 3.2 times that of PtRu(6-1)NTs and 5.5 times that of PtRu/C. As a result of the enhanced specific activity and increased ECSA, PtRu(4-1)/CuNWs show a mass activity comparable to PtRu/C in the potential region of 0.4−0.6 V, and 2.5 times that of PtRu/C at peak potential (Figure 4b). Chronoamperometry curves of PtRu(6-1)NTs, PtRu(4-1)/CuNWs, and PtRu/C were recorded at 0.6 V vs RHE for 1800 s to evaluate the stability of the catalysts (Figure 4c). The currents decayed rapidly initially due to the poisoning of the surface by strongly adsorbed intermediates. For easier comparison of the stability of the catalysts, the currents in the chronoamperometry curves were normalized to their initial current (Figure S10). In the initial 200 s, PtRu(4-1)/CuNWs showed the lowest decaying rate, followed by PtRu(6-1)NTs and PtRu/C. Over longer period of time, a relatively higher current was observed on PtRu(6-1)NTs and PtRu(4-1)/CuNWs than PtRu/C, indicating their better stability. The

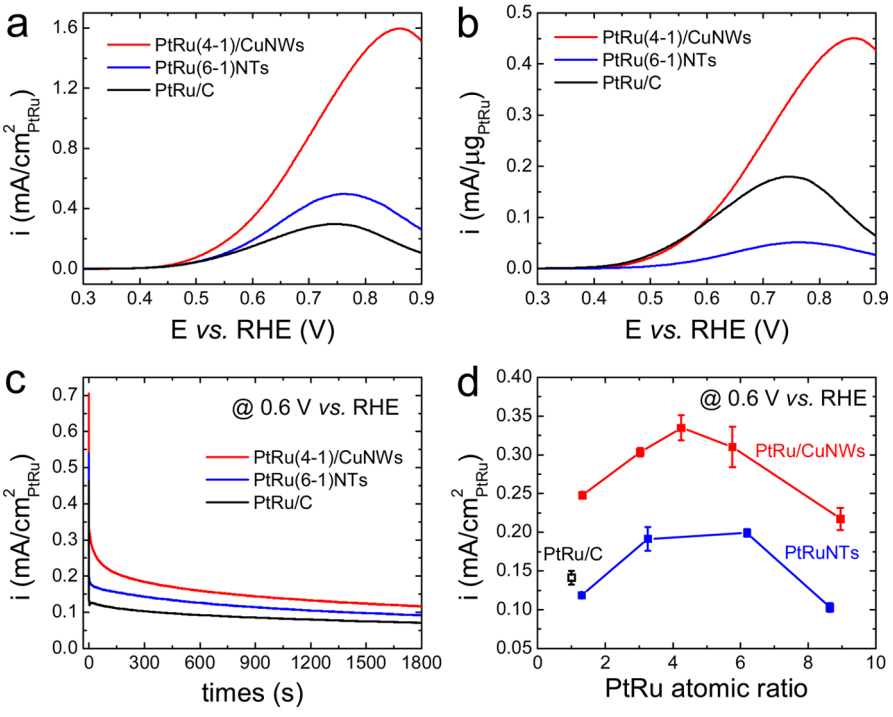

Figure 4. Cyclic voltammogram (forward scan) of PtRu(4-1)/CuNWs, PtRu(6-1)NTs, and PtRu/C in terms of (a) specific activity and (b) mass activity. Test condition: 0.1 M $HClO_4$, 1 M MeOH, Ar, scanning rate: 5 mV/s. (c) Chronoamperometry of PtRu(4-1)/CuNWs, PtRu(6-1)NTs, and PtRu/C measured at 0.6 V vs RHE for 1800 s. (d) Plot of specific MOR activities at 0.6 V vs RHE as a function of PtRu atomic ratio on PtRu/CuNWs, PtRuNTs and PtRu/C. Error bars represents three independent measurements of each sample.

DOI: 10.1021/cs501449y
ACS Catal. 2015, 5, 1468−1474

stability of core Cu is important for the application of PtRu/CuNWs in fuel cells since dissolution of Cu is detrimental to the stability of proton exchange membrane (e.g., Nafion). Our previous study on a similar structure Pt coated CuNWs annealed at 250 °C (PtCu-250) showed minimal Cu dissolution after accelerated durability test via cycling between 0.6 to 1.1 V vs RHE at 50 mV/s in 0.1 M $HClO_4$ for 30 000 cycles once the sample was predealloyed,[39] indicating that the core Cu is well protected.

PtRu compositional effect was clearly observed on PtRu/CuNWs and PtRuNTs. The specific MOR activities at 0.6 V vs RHE of PtRuNTs and PtRu/CuNWs with various PtRu ratios were obtained from their cyclic voltammograms (Figure S11) and were plotted as a function of PtRu atomic ratio measured from EDX (Figure 4d). Similar trends were obtained on both PtRuNTs and PtRu/CuNWs: a PtRu atomic ratio of about 4 gave the highest specific activity. The optimum PtRu atomic ratios for MOR from various studies are summarized in Table S2. Although the optimum PtRu atomic ratio range from 1 to 3 in bulk composition has been reported (Table S2), the work from Gasteiger et al. showed that PtRu alloys with a surface composition of 10 at. % Ru has the highest activity.[40]The discrepancy in the optimal PtRu ratio may be attributed to the difference between the surface PtRu composition and the bulk composition, as well as the difference in preparation methods of each catalyst.

X-ray photoemission spectroscopy (XPS) was used to determine the surface compositions as well as the electronic states of PtRuNTs, PtRu/CuNWs, and PtRu/C (Figure S14 and S15). The surface compositions of Pt, Ru, and Cu measured from XPS are listed in Table S1. Smaller PtRu surface atomic ratio was obtained than PtRu bulk atomic ratio on PtRu(6-1)NTs and all PtRu/CuNWs, indicating the surface enrichment of Ru during galvanic displacement reaction. Because $PtCl_6^{2-}$ has a higher redox potential (0.742 V) than Ru^{3+} (0.616 V), the larger driving force between Pt and Cu will lead to a more preferential displacement of Cu with Pt. Therefore, CuNWs will be displaced by Pt and Ru in a PtRu ratio higher than the stoichiometric PtRu ratio in the precursor initially and lower than the stoichiometric value in the final stage, resulting in a higher Ru content in the surface. The enrichment of Ru on the surface can also be validated from the elemental mapping of Ru in PtRu(6-1)NTs and PtRu(4-1)/CuNWs (Figure 1e,f and Figure S4, S7).

The optimal surface PtRu atomic ratios of PtRuNTs and PtRu/CuNWs, which are around 1.10 and 1.35, are quite different from that reported by Gasteiger et al., which is 9.[40] Because adsorption of methanol on Pt require three adjacent Pt sites, according to a model based on bifunctional mechanism, a surface structure having one Ru atom neighboring three Pt sites represents optimum geometry, and it was calculated that 10 at. % Ru maximizes this configuration, supporting Gasteiger's report. However, this model fails to capture the electronic effect on Pt induced by Ru. The presence of Cu in PtRuNTs and PtRu/CuNWs might also alter the optimum PtRu ratio due to the electronic effect on Pt induced by Cu. Additionally, the preparation methods of the catalysts will influence the optimum PtRu atomic ratio, considering different preparation methods could lead to catalysts with various degrees of alloying, morphologies, and so forth. Watanabe et al. reported an optimal surface PtRu atomic ratio of 1 for PtRu alloy and Ru decorated Pt disk,[19] which is similar to that in our case.

To understand the role of the one-dimensional structure, we also synthesized PtNTs and Pt/CuNWs using the same methods as in the synthesis of PtRuNTs and PtRu/CuNWs without adding Ru precursors. Their MOR activities were investigated and compared with that of Pt disk and TKK Pt/C (Figure S13a). PtNTs show a specific MOR activity similar to Pt disk, but much higher than Pt/C, which agrees with the results reported by Alia et al.[9] From CO-stripping experiments (Figure S13b), similar CO-stripping peak potentials are observed for PtNTs and Pt disk at about 0.70 V, whereas Pt/C exhibited a peak at a much higher potential (about 0.83 V). Particle size effects on MOR for Pt has been investigated by various groups,[41−45] and the MOR specific activity was found to decrease as Pt nanoparticle size decreases. With this trend, we expect that bulk platinum will have the highest MOR activity, which explains why PtNTs with extended surfaces show MOR activity similar to the Pt disk and much higher than Pt nanoparticles. Meanwhile, the CO-stripping peak position is strongly dependent on surface facets: for low index Pt facets, the CO-stripping peak occurs at 0.87 V for Pt(111),[46] 0.7 V for Pt(110),[47] and 0.79 V for Pt(100).[48] PtNTs show the same CO-stripping peak potential as Pt(110), indicating PtNTs might preferentially expose Pt(110) facet on their surface, which is known to possess the highest MOR activity among the three low index facets.[6] Although step or defect sites are beneficial for enhancing MOR activity on Pt,[49] their promotional effect may not be as effective as exposing the most active surface. Analogously, we hypothesize that PtRuNTs achieved a higher activity than PtRu/C due to their extended surfaces.

Figure 5 represents the Pt 4f and Ru $3p_{3/2}$ XPS spectra for PtRu/C, PtRu(6-1)NTs, and PtRu(4-1)/CuNWs. The Pt 4f

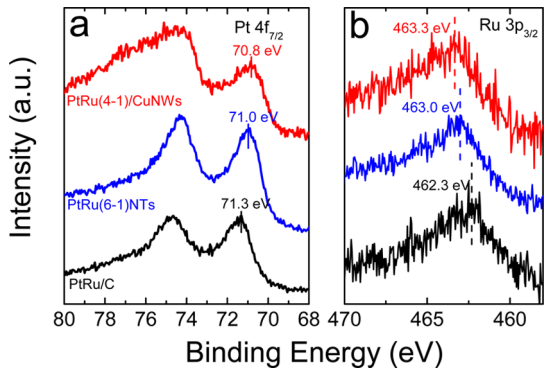

Figure 5. XPS spectra of PtRu/C, PtRu(6-1)NTs, and PtRu(4-1)/CuNWs: (a) Pt 4f, (b) Ru $3p_{3/2}$.

spectra forms doublet peaks Pt $4f_{7/2}$ and Pt $4f_{5/2}$ due to spin orbit coupling, and the intensities of 7/2 and 5/2 peaks are 4:3 (Figure 5a, Figures S14 and S15). PtRuNTs have peaks at binding energy (BE) values of 71.0 and 74.3 eV assigned to Pt(0) species and peaks with BE values of 73.1 and 76.4 eV attributed to Pt(II) species (Figure S14a). For PtRu/CuNWs, there exist Cu $3p_{3/2}$ and Cu $3p_{1/2}$ peaks in the Pt 4f region, causing the broadening of the peak at BE of about 74 eV (Figure 5a and Figure S15).

The Pt 4f binding energy decreased in order of PtRu/C > PtRu(6-1)NTs > PtRu(4-1)/CuNWs (Figure 5a), whereas the Ru 3p binding energy followed the exact opposite trend (Figure 5b), indicating that Pt obtains more electrons from Ru from PtRu(4-1)/CuNWs to PtRu(6-1)NTs to PtRu/C. This is consistent with the fact that Pt has a larger electronegativity

DOI: 10.1021/cs501449y
ACS Catal. 2015, 5, 1468−1474

that Ru (2.28 vs 2.20). Additionally, the surface copper in PtRuNTs and PtRu/CuNWs could also contribute electrons to Pt due to its even lower electronegativity (1.90). The core-level shifts in XPS are usually correlated with changes in the d-band center. However, while some conclude that an upshift of binding energy corresponds to a lower d-band center (i.e., with d-band center further away from the Fermi level),[17,50] others report the opposite correlation—that a downshift of binding energy is indicative of a lower d-band center.[51−53] This discrepancy is discussed by Poh et al.—that the XPS core level shift is affected by several factors and both correlations are possible.[50] They finally explained the trend of the d-band center shift based on the existence of charge transfer from metals with low work function to metals with higher work function, leading to the rise of Fermi level of the metal with higher work function, which corresponds to the downshift of d-band center. In our case, we observed more electron transfer from Ru or Cu to Pt in PtRu/CuNWs than PtRuNTs and PtRu/C, hence the d-band center of PtRu/CuNWs will be the lowest among the three samples. The lower d-band center is usually related with a weaker binding of the adsorbate to the metal,[54] and in this case, the poisoning intermediate CO to Pt. The early onset of CO monolayer oxidation in CO-stripping measurements on PtRu/CuNWs (0.28 V) compared with that of PtRuNTs (0.3 V) and PtRu/C (0.32 V) (inset of Figure 3), is another strong evidence of weaker Pt-CO binding in PtRu/CuNWs.

CONCLUSION

In conclusion, we have synthesized PtRuNTs and PtRu/CuNWs via galvanic displacement reaction using CuNWs as template and presented their efficient catalytic activities of electro-oxidation of methanol. The compositional effect study show an optimal PtRu bulkatomic ratio of about 4 and surface atomic ratio of about 1 for both PtRuNTs and PtRu/CuNWs. Enhanced specific MOR activities were observed on PtRuNTs and PtRu/CuNWs compared with the benchmark PtRu/C, with specific activity in the order of PtRu/CuNWs > PtRuNTs > PtRu/C. The improvement of specific activity of PtRuNTs might be partially attributed from the extended surface of their intrinsic nanotube structure. The XPS measurement of PtRu(4-1)/CuNWs, PtRu(6-1)NTs and PtRu/C revealed a stronger electron transfer from Ru to Pt in PtRu(4-1)/CuNWs than PtRu(6-1)NTs followed by PtRu/C, which corresponds to its lower d-band center. Meanwhile, the modification of the d-band center can lead to a weaker bonding of Pt to the poisoning intermediate CO, resulting in improved specific MOR activity of PtRu(4-1)/CuNWs. However, a smaller mass MOR activity was obtained on PtRuNTs compared with PtRu/C caused by their small ECSA. PtRu(4-1)/CuNWs achieved a comparable mass activity at lower potential range (<0.6 V vs RHE) and a much higher mass activity at potential larger than 0.6 V vs RHE, ascribed to their improved specific activity as well as increased ECSA. We believe that PtRu/CuNWs with 1D morphology will be a promising anode catalyst for DMFCs due to their good mass activity and their potential benefit in improving mass transport.

ASSOCIATED CONTENT

Supporting Information

The following file is available free of charge on the ACS Publications website at DOI: 10.1021/cs501449y.

Elemental compositions of samples measured by EDX and XPS, SEM and TEM images of CuNWs, SEM, EDX and HAADF-STEM of PtRuNTs and PtRu/CuNWs, cyclic voltammograms of PtRu/C, PtRuNTs and PtRu/CuNWs, XPS of PtRuNTs and PtRu/CuNWs (PDF)

AUTHOR INFORMATION

Corresponding Author

*E-mail: yanys@udel.edu. Fax: 302.831.2582.

Notes

The authors declare no competing financial interest.

ACKNOWLEDGMENTS

This work was financially supported by the U.S. Department of Energy through the Fuel Cell Technologies Program under No. DE-AC36-08-NA25396 with the Los Alamos National Laboratory.

REFERENCES

(1) Aricò, A. S.; Baglio, V.; Antonucci, V. In *Electrocatalysis of Direct Methanol Fuel Cells*; Wiley-VCH Verlag GmbH & Co. KGaA: Weinheim, 2009; pp 1−78.
(2) Hamnett, A. In *Handbook of Fuel Cells*; Vielstich, W., Lamm, A., Gasteiger, H. A., Eds.; John Wiley & Sons, Ltd: London, 2010; Vol. *1*, pp 305−322.
(3) Iwasita, T. In *Handbook of Fuel Cells*; Gasteiger, H. A., Kocha, S. S., Sompali, B., Wagner, F. T., Eds.; John Wiley & Sons, Ltd: London, 2010; Vol. *2*, pp 603−624.
(4) Wasmus, S.; Küver, A. *J. Electroanal. Chem.* **1999**, *461*, 14−31.
(5) Liu, H. S.; Song, C. J.; Zhang, L.; Zhang, J. J.; Wang, H. J.; Wilkinson, D. P. *J. Power Sources* **2006**, *155*, 95−110.
(6) Herrero, E.; Franaszczuk, K.; Wieckowski, A. *J. Phys. Chem.* **1994**, *98*, 5074−5083.
(7) Koenigsmann, C.; Wong, S. S. *Energy Environ. Sci.* **2011**, *4*, 1161−1176.
(8) Bi, Y.; Lu, G. *Electrochem. Commun.* **2009**, *11*, 45−49.
(9) Alia, S. M.; Zhang, G.; Kisailus, D.; Li, D.; Gu, S.; Jensen, K.; Yan, Y. *Adv. Funct. Mater.* **2010**, *20*, 3742−3746.
(10) Ruan, L.; Zhu, E.; Chen, Y.; Lin, Z.; Huang, X.; Duan, X.; Huang, Y. *Angew. Chem., Int. Ed.* **2013**, *52*, 12577−12581.
(11) Cui, C.-H.; Li, H.-H.; Yu, S.-H. *Chem. Sci.* **2011**, *2*, 1611−1614.
(12) Ding, L.-X.; Wang, A.-L.; Li, G.-R.; Liu, Z.-Q.; Zhao, W.-X.; Su, C.-Y.; Tong, Y.-X. *J. Am. Chem. Soc.* **2012**, *134*, 5730−5733.
(13) Kim, S. M.; Liu, L.; Cho, S. H.; Jang, H. Y.; Park, S. *J. Mater. Chem. A* **2013**, *1*, 15252−15257.
(14) Guo, S.; Zhang, S.; Sun, X.; Sun, S. *J. Am. Chem. Soc.* **2011**, *133*, 15354−15357.
(15) Choi, W. C.; Woo, S. I. *J. Power Sources* **2003**, *124*, 420−425.
(16) Li, B.; Higgins, D. C.; Zhu, S.; Li, H.; Wang, H.; Ma, J.; Chen, Z. *Catal. Commun.* **2012**, *18*, 51−54.
(17) Li, H.-H.; Zhao, S.; Gong, M.; Cui, C.-H.; He, D.; Liang, H.-W.; Wu, L.; Yu, S.-H. *Angew. Chem., Int. Ed.* **2013**, *52*, 7472−7476.
(18) Hong, W.; Wang, J.; Wang, E. *Small* **2014**, *10*, 3262−3265.
(19) Watanabe, M.; Motoo, S. *J. Electroanal. Chem.* **1975**, *60*, 267−273.
(20) Marković, N. M.; Gasteiger, H. A.; Ross, P. N., Jr; Jiang, X.; Villegas, I.; Weaver, M. J. *Electrochim. Acta* **1995**, *40*, 91−98.
(21) Frelink, T.; Visscher, W.; van Veen, J. A. R. *Surf. Sci.* **1995**, *335*, 353−360.
(22) Zhao, G.-Y.; Xu, C.-L.; Guo, D.-J.; Li, H.; Li, H.-L. *J. Power Sources* **2006**, *162*, 492−496.
(23) Minch, R.; Es-Souni, M. *Chem. Commun.* **2011**, *47*, 6284−6286.
(24) Chen, Z.; Waje, M.; Li, W.; Yan, Y. *Angew. Chem., Int. Ed.* **2007**, *46*, 4060−4063.
(25) Sun, Y. *Nanoscale* **2010**, *2*, 1626−1642.

DOI: 10.1021/cs501449y
ACS Catal. 2015, 5, 1468−1474

(26) Alia, S. M.; Jensen, K. O.; Pivovar, B. S.; Yan, Y. *ACS Catal.* **2012**, *2*, 858−863.
(27) Lu, X.; McKiernan, M.; Peng, Z.; Lee, E. P.; Yang, H.; Xia, Y. *Sci. Adv. Mater.* **2010**, *2*, 413−420.
(28) Mohl, M.; Dobo, D.; Kukovecz, A.; Konya, Z.; Kordas, K.; Wei, J.; Vajtai, R.; Ajayan, P. M. *J. Phys. Chem. C* **2011**, *115*, 9403−9409.
(29) Li, H.-H.; Cui, C.-H.; Zhao, S.; Yao, H.-B.; Gao, M.-R.; Fan, F.-J.; Yu, S.-H. *Adv. Energy Mater.* **2012**, *2*, 1182−1187.
(30) Alia, S. M.; Jensen, K.; Contreras, C.; Garzon, F.; Pivovar, B.; Yan, Y. *ACS Catal.* **2013**, *3*, 358−362.
(31) Zhu, C.; Guo, S.; Dong, S. *J. Mater. Chem.* **2012**, *22*, 14851−14855.
(32) Zhu, C.; Guo, S.; Dong, S. *Adv. Mater.* **2012**, *24*, 2326−2331.
(33) Chang, Y.; Lye, M. L.; Zeng, H. C. *Langmuir* **2005**, *21*, 3746−3748.
(34) Fan, H. J.; Gösele, U.; Zacharias, M. *Small* **2007**, *3*, 1660−1671.
(35) Wang, J. X.; Ma, C.; Choi, Y.; Su, D.; Zhu, Y.; Liu, P.; Si, R.; Vukmirovic, M. B.; Zhang, Y.; Adzic, R. R. *J. Am. Chem. Soc.* **2011**, *133*, 13551−13557.
(36) Xia, X.; Wang, Y.; Ruditskiy, A.; Xia, Y. *Adv. Mater.* **2013**, *25*, 6313−6333.
(37) Kinoshita, K.; Ross, P. N. *J. Electroanal. Chem.* **1977**, *78*, 313−318.
(38) Schmidt, T. J.; Noeske, M.; Gasteiger, H. A.; Behm, R. J.; Britz, P.; Brijoux, W.; Bönnemann, H. *Langmuir* **1997**, *13*, 2591−2595.
(39) Wittkopf, J. A.; Zheng, J.; Yan, Y. *ACS Catal.* **2014**, *4*, 3145−3151.
(40) Gasteiger, H. A.; Markovic, N.; Ross, P. N.; Cairns, E. J. *J. Phys. Chem.* **1993**, *97*, 12020−12029.
(41) Takasu, Y.; Fujii, Y.; Matsuda, Y. *Bull. Chem. Soc. Jpn.* **1986**, *59*, 3973−3974.
(42) Yahikozawa, K.; Fujii, Y.; Matsuda, Y.; Nishimura, K.; Takasu, Y. *Electrochim. Acta* **1991**, *36*, 973−978.
(43) Kabbabi, A.; Gloaguen, F.; Andolfatto, F.; Durand, R. *J. Electroanal. Chem.* **1994**, *373*, 251−254.
(44) Frelink, T.; Visscher, W.; Vanveen, J. A. R. *J. Electroanal. Chem.* **1995**, *382*, 65−72.
(45) Takasu, Y.; Iwazaki, T.; Sugimoto, W.; Murakami, Y. *Electrochem. Commun.* **2000**, *2*, 671−674.
(46) Gasteiger, H. A.; Markovic, N.; Ross, P. N.; Cairns, E. J. *J. Phys. Chem.* **1994**, *98*, 617−625.
(47) Hayden, B. E.; Murray, A. J.; Parsons, R.; Pegg, D. J. *J. Electroanal. Chem.* **1996**, *409*, 51−63.
(48) Herrero, E.; Feliu, J. M.; Aldaz, A. *J. Electroanal. Chem.* **1994**, *368*, 101−108.
(49) Lee, S. W.; Chen, S.; Sheng, W.; Yabuuchi, N.; Kim, Y.-T.; Mitani, T.; Vescovo, E.; Shao-Horn, Y. *J. Am. Chem. Soc.* **2009**, *131*, 15669−15677.
(50) Poh, C. K.; Tian, Z.; Gao, J.; Liu, Z.; Lin, J.; Feng, Y. P.; Su, F. *J. Mater. Chem.* **2012**, *22*, 13643−13652.
(51) Wang, S.; Yang, F.; Jiang, S. P.; Chen, S.; Wang, X. *Electrochem. Commun.* **2010**, *12*, 1646−1649.
(52) Mao, X.; Yang, L.; Yang, J.; Key, J.; Ji, S.; Wang, H.; Wang, R. *J. Electrochem. Soc.* **2013**, *160*, H219−H223.
(53) Johansson, A.-C.; Larsen, J. V.; Verheijen, M. A.; Haugshøj, K. B.; Clausen, H. F.; Kessels, W. M. M.; Christensen, L. H.; Thomsen, E. V. *J. Catal.* **2014**, *311*, 481−486.
(54) Hammer, B.; Nørskov, J. K. In *Adv. Catal.*; Bruce, C. Gates, H. K., Ed.; Academic Press: San Diego, CA, 2000; Vol. *45*, pp 71−129.

DOI: 10.1021/cs501449y
ACS Catal. 2015, 5, 1468−1474